Supporting Information for "Variational inference of ice shelf rheology with physics-informed machine learning"

B. Riel[1,2], B. Minchew[2]

[1]School of Earth Sciences, Zhejiang University, Hangzhou, China

[2]Department of Earth, Atmospheric and Planetary Sciences, Massachusetts Institute of Technology, Cambridge, MA, USA

Contents of this file

1. Figures S1 to S11

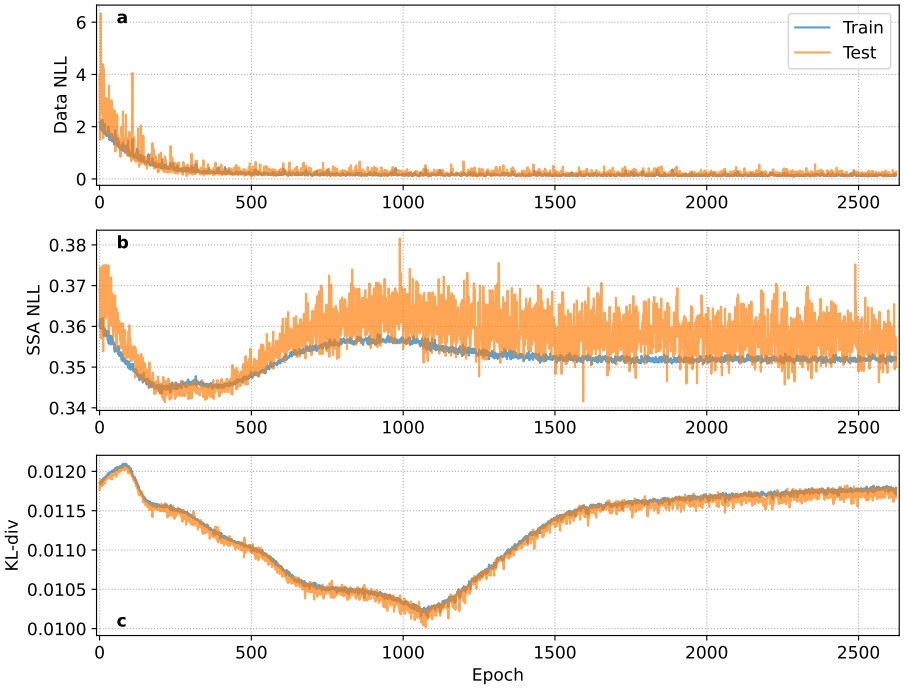

Figure S1. Training history for 1D synthetic ice shelf for different components of the ELBO objective function. For all plots, blue lines correspond to the loss values for the training data while the orange lines are the loss values for the test data. a) Negative data log-likelihood loss for measuring reconstruction accuracy. b) Negative SSA residual log-likelihood loss for measuring consistency with SSA momentum balance. c) KL-divergence for measuring consistency between the variational posterior and prior distributions for the ice rigidity. Generally, training is terminated once all three losses show negligible changes.

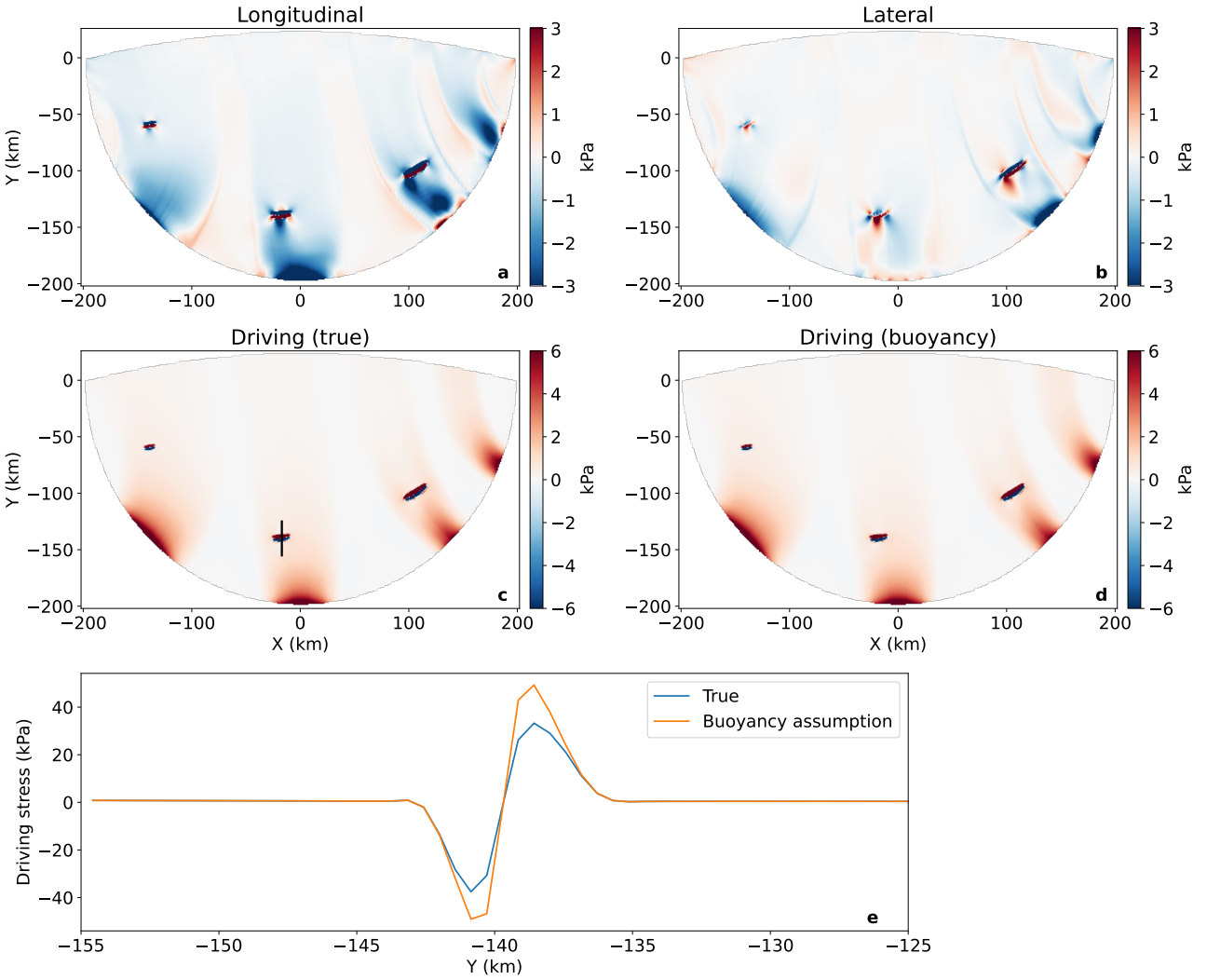

Figure S2. Components of SSA momentum balance for synthetic 2D ice shelf using noise-free velocities, ice thickness, and surface elevation. Individual terms in the 2D SSA momentum balance are projected into the along-flow direction to obtain longitudinal stress (a), lateral drag (b), driving stresses computed with true thickness and elevation (c), and driving stresses computed with thickness derived from assuming hydrostatic equilibrium (buoyancy) (d). In (e), a transect of driving stresses over a pinning point (shown by black line in (c)) indicates that assuming buoyancy over the entire ice shelf can lead to localized errors in driving stress over the pinning points where ice is grounded.

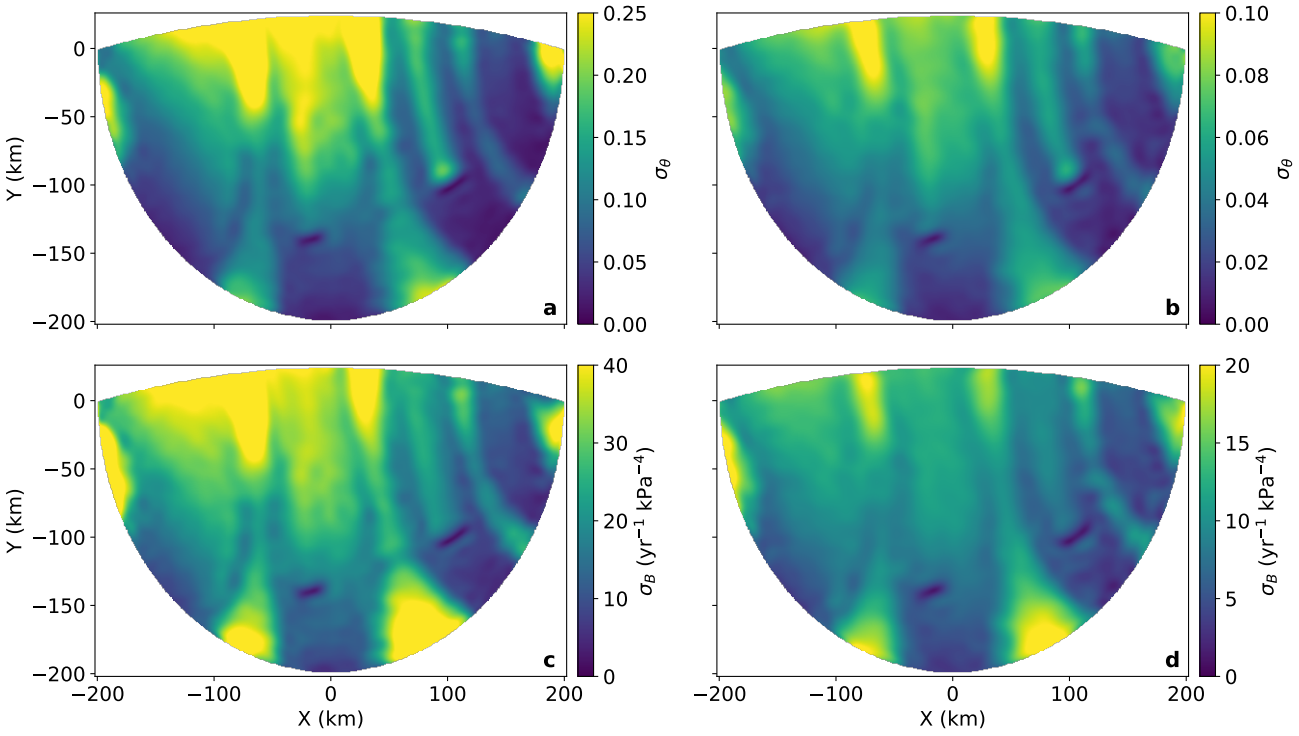

Figure S3. Posterior uncertainties for ice rigidity for synthetic 2D ice shelf. a) Uncertainty for normalized rigidity (θ) for a constant prior B_0. b) Uncertainty for θ using a spatially-varying B_0 obtained from a control-method inversion. c) Uncertainty for rigidity (B) for a constant prior. d) Uncertainty for B using a spatially-varying B_0 obtained from a control-method inversion. Note the change in color scales between the left and right panels. Using the inversion-estimated B as a prior, coupled with a reduction in prior variances, provides an avenue to reduce in uncertainties in inferred ice rigidity.

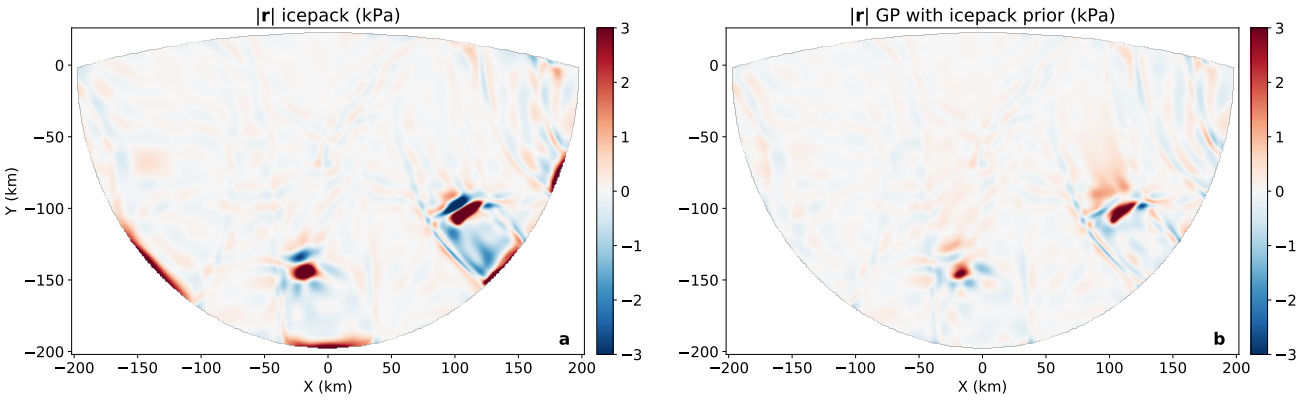

Figure S4. Comparison of magnitude of SSA residuals ($\|\mathbf{r}\| = \sqrt{r_x^2 + r_y^2}$) computed using ice rigidity from control method inversion (a) and mean of variational Gaussian Process (b). True ice velocity and thickness (as output from 2D simulations) are used to compute residuals. Note the larger residual values near the grounding line and upstream of the pinning points for the control method inversion as compared to the variational Gaussian process.

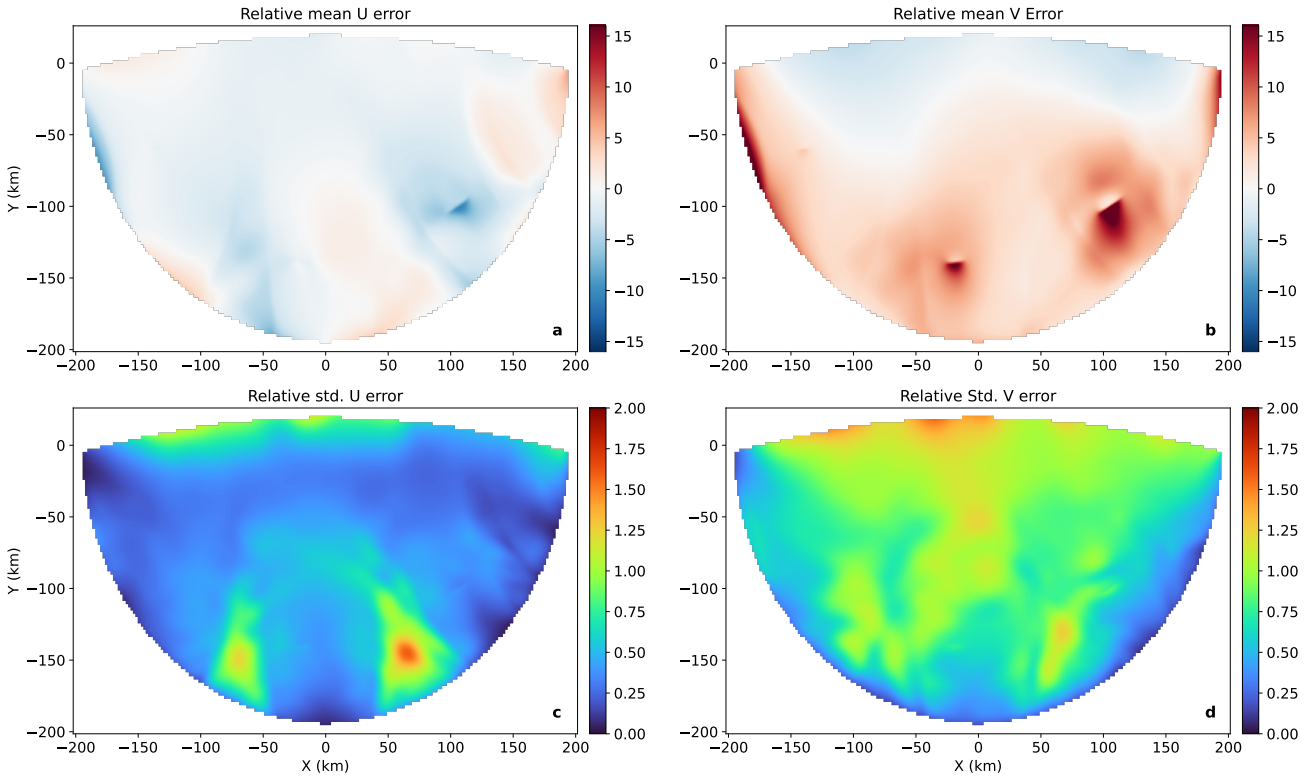

Figure S5. Summary of forward model error statistics using samples of rigidity B generated by variational Gaussian Process. Each B sample is used to predict the two velocity components, U and V. The error between the predicted and true velocity components is then computed and normalized to the true velocity magnitude. The top panels show the mean percentage error while the bottom panels show the standard deviation in percentage error. Mean velocity errors are concentrated near the pinning points. Otherwise, errors are generally below 5%.

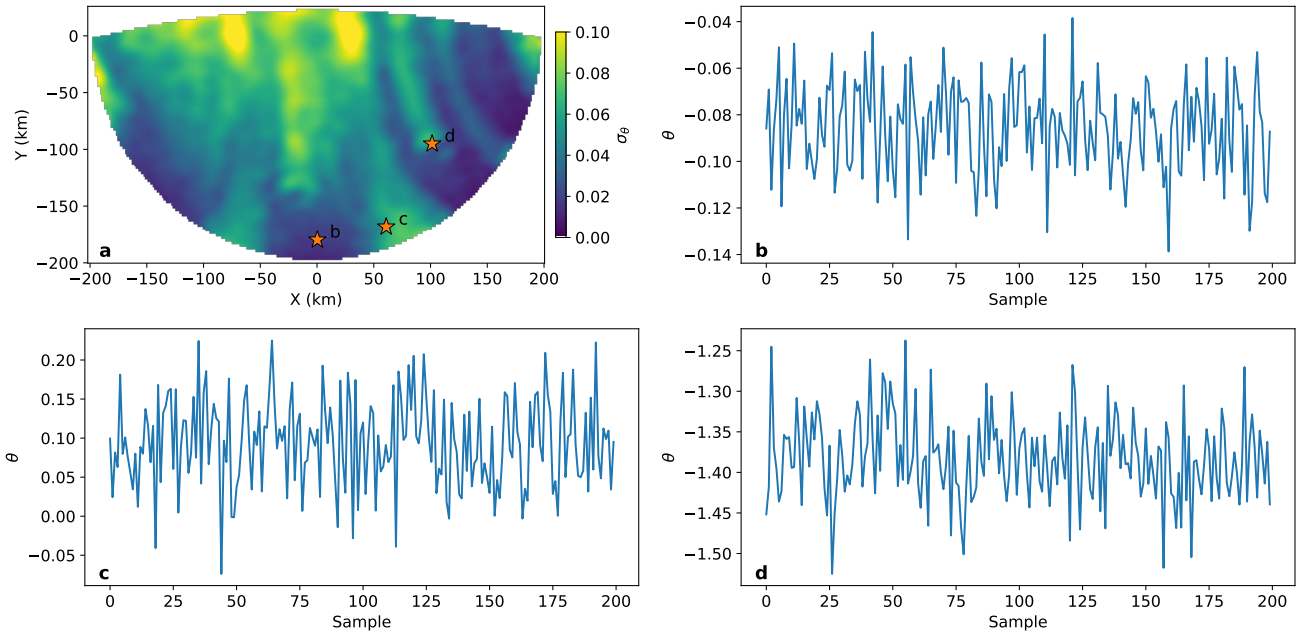

Figure S6. Random samples from variational posterior $q(\theta)$ of synthetic 2D ice shelf using Gibbs sampling algorithm. A map of the standard deviation of the θ samples is shown in (a), along with the locations corresponding to the trace plots in (b)-(d).

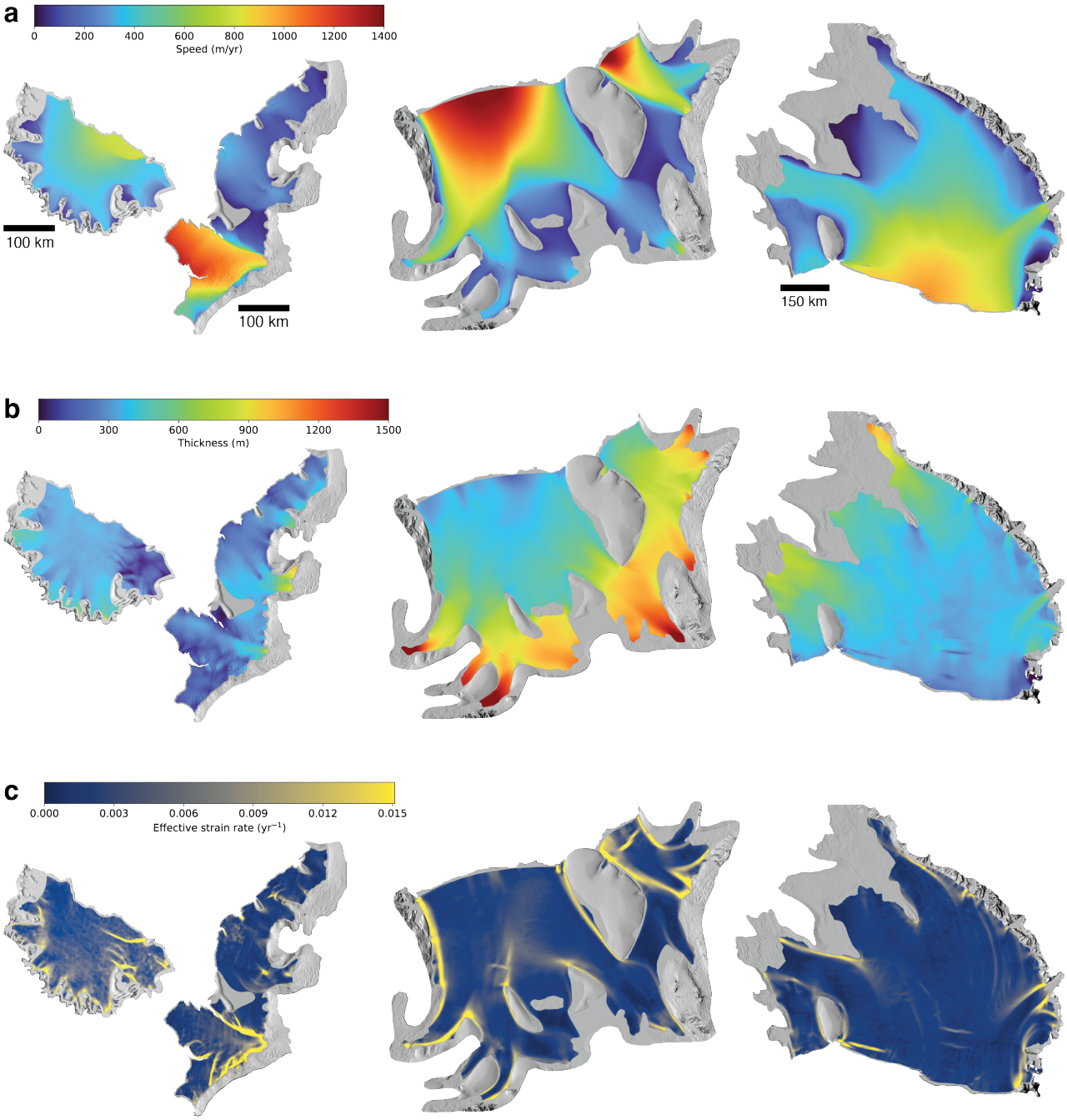

Figure S7. Ice flow speed, thickness, and strain-rate for select West Antarctic Ice Shelves.

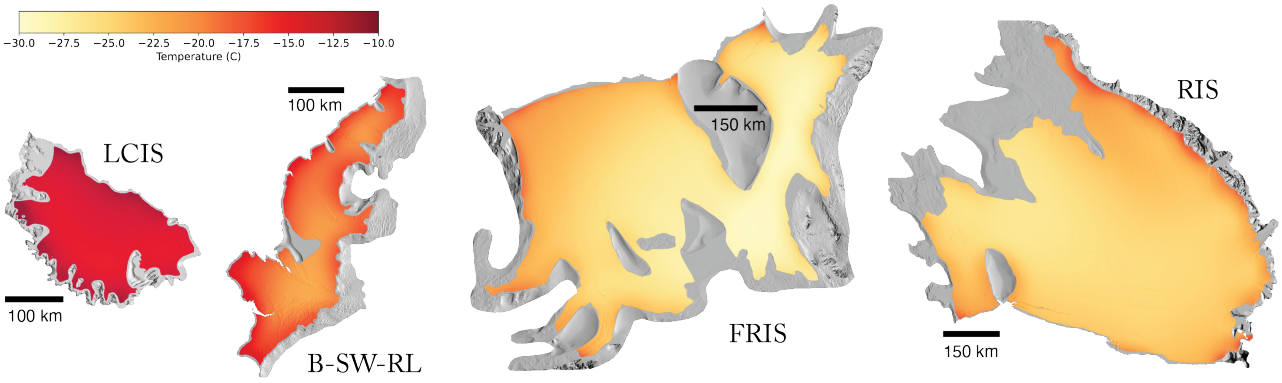

Figure S8. Modeled surface temperature (2 m) for West Antarctic Ice Shelves derived from the regional atmospheric climate model (RACMO2) re-gridded to a 500 meter grid spacing. RACMO2 data were downloaded from `https://doi.org/10.5281/zenodo.6602723`.

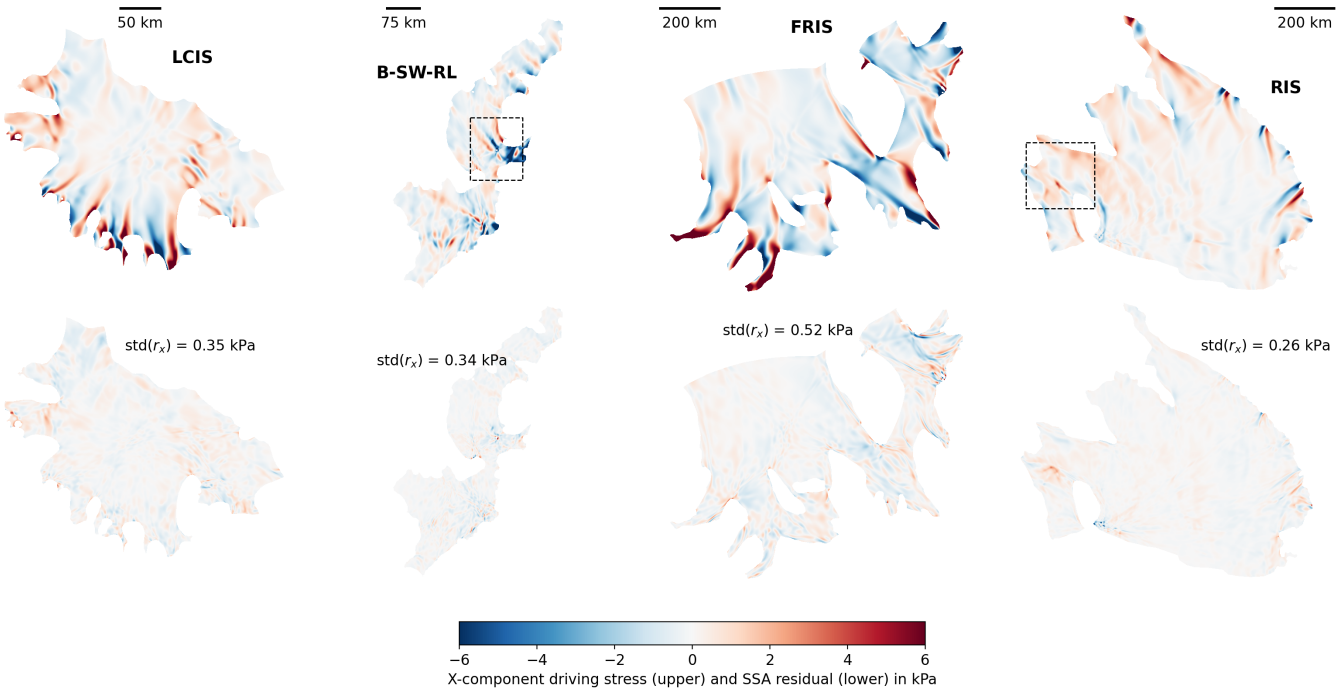

Figure S9. Reconstructed driving stress (upper panels) and x-component SSA residual r_x (lower panels) for West Antarctic Ice Shelves (abbreviations defined in main text). Driving stress is computed from neural network-predicted ice thickness, $\hat{h}$, and r_x is computed from the mean rigidity predicted from the variational Gaussian Process. Generally, medium- to long-wavelength components of the SSA momentum balance are well-modeled by the rigidity field. Near certain fine-resolution features like rifts and shear margins, residuals are slightly larger due to oversmoothing of the rigidity field. Over pinning points, residuals are also higher due to un-modeled basal drag. Black dashed rectangles correspond to the regions shown in Figure S11.

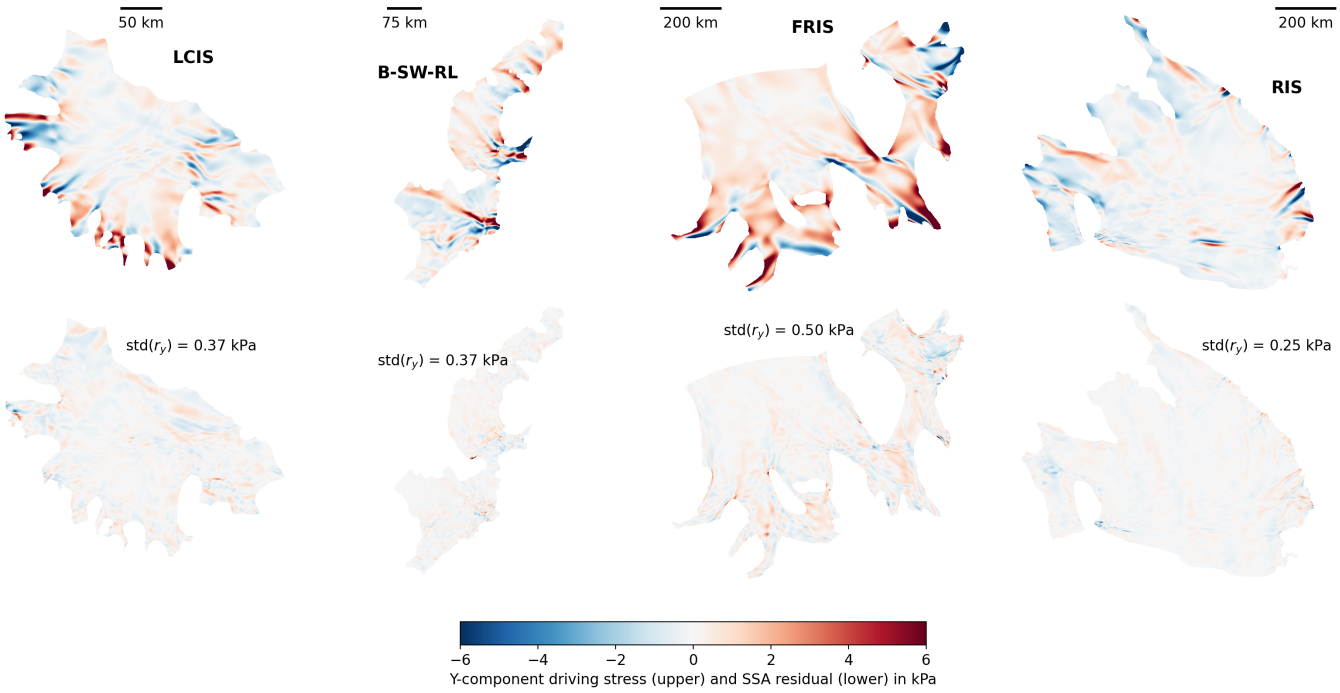

Figure S10. Same as Figure S9 but in the y-direction.

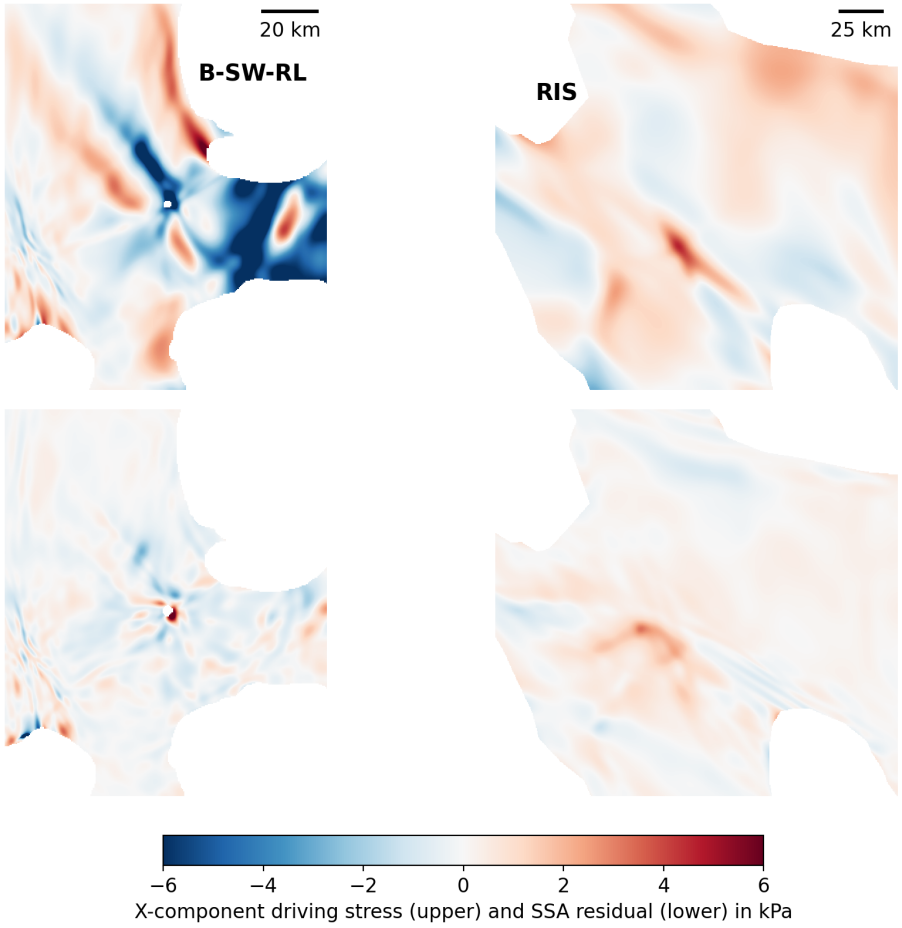

Figure S11. Zoomed-in view of x-component driving stress (upper) and SSA residuals (lower) for B-SW-RL and RIS (extent shown in Figure S9).